PRE-PRINT:

Maritan, L., Gravagna, E., Cavazzini, G., Zerboni, A., Mazzoli, C., Grifa, C., Mercurio, M., Mohamed, A.A., Usai, D., Salvatori, S., *Nile River clayey materials in Sudan: chemical and isotope analysis as reference data for ancient pottery provenance studies*. Quaternary International. https://doi.org/10.1016/j.quaint.2021.05.009

Nile River clayey materials in Sudan: chemical and isotope analysis as reference data for ancient pottery provenance studies

Lara Maritan[1,*], Elisa Gravagna[1], Giancarlo Cavazzini[2], Andrea Zerboni[3], Claudio Mazzoli[1], Celestino Grifa[4], Mariano Mercurio[4], Abdelrahman Ali Mohamed[5], Donatella Usai[6], Sandro Salvatori[6]

[1]Department of Geosciences, University of Padova, Via Gradenigo 6, I-35131 Padova, Italy

[2]Institute of Geosciences and Georesources, CNR, Via Via Gradenigo 6, I-35131 Padova, Italy

[3]Dipartimento di Scienze della Terra "A. Desio", Università degli studi di Milano, Via L. Mangiagalli 34, I-20133 Milano, Italy

[4]Department of Science and Technology, University of Sannio, Via De Sanctis snc, I-82100 Benevento, Italy

[5]National Corporation for Antiquities and Museums (NCAM), Khartoum, Sudan

[6]Centro Studi Sudanesi e Sub-Sahariani (CSSeS), Strada Canizzano 128/d, I-31100 Treviso, Italy

* Corresponding author

lara.maritan@unipd.it

Abstract

This research aims to define a chemical, mineralogical and strontium isotope database for clayey materials collected along the Nile River banks (White Nile, Blue Nile, Atbara and Main Nile Rivers) in Sudan, to be use for prehistoric and historic pottery provenance studies. The approach here adopted consists in using the clayey materials tout court, without any pre-treatment, such as the depuration from the sand- and silt-sized fractions, in order to maintain unaltered, the

mineralogical and geochemical features of the natural resources possibly available also in ancient times for the pottery production, thus avoiding any possible preparation bias. Results indicate that sediments along different section of the Nile River display characteristic geochemical and strontium isotopic signature, representing an important discrimination tool applied to ancient ceramics provenance and human mobility studies.

Keywords: Chemistry; Mineralogy; Sr isotopes; Clayey materials; Nile River; Provenance markers

1. Introduction

Pottery, raw materials and tools have been always intimately related to the inscrutable events of ancient populations, including daily life, death and relationships. The technology regarding pottery production and its development involves essentially three variables (clay, fire and need for containers) that are closely intertwined with a 'complex mix of ecological, historical, economic, and social factors that differed greatly among past human societies' (Hoopes and Barnett 1995). Specific environmental and social processes appear to be involved in the origin of pottery, since several locations sited far away attest that fired clay containers and their technology were well known since ancient times. The appearance of ceramic materials (broadly intended as fired clay) occurred in different moments in the various region of the world: around 26000 years BP in Europe (Verpoorte 2001; Budja 2006), 20000 BP in China (Xu et al. 2012), 16000 BP in Japan (Shelach 2012), 10000 BP in Africa (Huysecom et al. 2009; Jesse 2010) and 7500 BP in South America (Roosevelt et al. 1996). All these findings date back to a period still characterized by a non-sedentary way of life based on hunting, gathering and fishing.

Archaeological studies carried out in the last decades in central and northern Sudan (Usai 2021), indicate that this region has been intensively frequented by hunter-gatherer-fisher groups since the Mesolithic (since ~ mid 9500 BP). The numerous sites discovered, although in many cases stratigraphically disturbed by subsequent anthropic activities, show the use of technologically well-developed ceramic materials, an optimized exploitation of the natural resources and diversified foraging activities (Dal Sasso et al. 2014; Honegger 2014; Maritan et al. 2018; Usai 2021; Varadzinovà et al. 2017).

Increasing complexity and/or possible seasonal aggregations have been suggested for some hunter-gatherer groups that might have been associated with exchanges of products and/or technologies and might have occurred in specific and somehow sacred regions, related to some natural or environmental feature (Hommel 2016; Maritan et al. 2018). In order to attest relations among groups at different levels, many recent studies focus on provenance of prehistoric pottery as a key for tracing exchanges. To achieve a plausible answer to this archaeological issue, in addition to the study of pottery samples from different locations, it is necessary to build a reference collection of raw materials (i.e. clayey materials) belonging to the pertinent geographical area for comparison, and characterize them using the main and most suitable analytical techniques (Montana 2020; Hein and Kilikoglou 2020). At this regard, numerous approaches can be used, based mainly on petrographic and/or geochemical analysis, according to the ceramic paste (coarse and fine, respectively), although a multi-analytical study is always preferable for the possibility of disclosing different aspect of the ceramic production and to better assess their provenance and production technology (Maritan 2019; Gliozzo 2020).

In the last years various authors faced provenance of ancient pottery using isotope analysis, and in particular strontium isotope, which allowed to solve the origin of the geomaterials used (i.e. clayey material for the ceramic body, fluxes for glaze) since other methods such as the petrographic and bulk geochemical analysis were not conclusive (Li et al. 2006; Carter et al. 2011; Alex et al. 2012; Wiegand 2016; De Bonis et al. 2018; Shen et al. 2019; Makarona et al. 2016; Renson et al. 2021; Kibaroglu et al. 2019).

In the interesting geographic and archaeological context represented by Sudan, a reference data base of natural resources for the ceramic production represents an important tool to properly study ancient productions and to constrain possible pottery trades between communities (from the Mesolithic up to the more recent periods) along its main communication route: the Nile valley. Previous studies (Garzanti et al. 2006, 2015; Padoan et al. 2011; Woodward et al. 2015; Talbot et al. 2000) have explored the petrographic, mineralogical and geochemical composition of Nile sediments and those of some of its tributaries. However, in these works the statistics is quite limited, especially for central Sudan, and are excluded confluence areas, in which the geomorphological situation is complex, also in relation to their hydrographic evolution over time (Williams et al. 2015). Moreover, in these papers the authors have chosen to consider the coarse and fine (< 62 μm or < 40 μm) fractions of the deposits separately, which hardly correspond to the materials actually collected by the ancient potters, presumably represented by a sandy-silty clay.

In ancient ceramic production, especially in prehistoric but also in historic periods, any possible preparation of the clay material (levigation or tempering) was carried out according to the potters' skills and not by using the sophisticated separation methods as those available in modern laboratories (Eramo 2020).

Therefore, in order to produce an adequate chemical, mineralogical and Sr isotope reference database able to provide constraints in studies on ancient pottery productions and sourcing areas, an extensive sampling campaign has been carried out along the Nile River in the Sudanese territory, and the collected samples analyzed tout-court. Moreover, the data here produced have wider archaeological and anthropological implications, because can represent a further tool to investigate human mobility along the Nile River valley and between the Nile River and the arid regions at its margins.

2. General setting on the Nile River and geology of Sudan

The Nile River (and its drainage system) is a mega-river flowing in East Africa from south of the Equator into the Mediterranean Sea (Williams and Faure 1980; Woodward 2007; Macklin et al. 2015; Zerboni et al. in press). The Nile basin is the world's second largest world river basin and, as summarized by Woodward et al. (2007) it crosses a variety of environmental contexts and terrains including: the volcanic highlands of Ethiopia and Eritrea, the swamps of the Sudd, the ancient Nubian shield, the desert corridor between Khartoum and Cairo, the coastal zone of the Mediterranean shores. The evolution of the Nile drainage network depends on an array of triggering factors, including regional tectonic and volcanic processes and cyclical variations in erosion and sedimentation rates. The latter mostly depends on sea level changes and major Quaternary climate and land cover changes (Said 1981; Talbot and Williams 2009; Williams and Faure 1980; Woodward et al. 2015; Siam and Eltahir 2017). The drainage basin of the Nile River and major tributaries includes several sub-catchments: the White Nile, the Blue Nile, the Atbara, and the desert Nile (Main Nile). Each of the sub-catchments drain specific geological bedrocks and its headwater is fed by different water sources, therefore their loads and deposits have specific sedimentological, mineralogical and geochemical properties (Williams et al., 2000). A major implication of this fact is that the composition of sediments along the Nile River vary in correspondence of the insertion of each affluent to the main stream.

The geology of Sudan is extremely differentiated with a variety of metamorphic, igneous and sedimentary rocks (Figure 1). Its whole evolution is related to dynamic of the East Africa – Red Sea Rift System (Adamson and Williams 1980). Along the Sudanese Nile Valley, the most widespread formations are those belonging to the Pre-Cambrian basement complex (also defined as Pan-African basement), consisting in igneous (mainly syenite and granite, but also diorite, gabbro and rhyolite), high-grade metamorphic (mainly metapelites, orthogneisses and migmatites) and sedimentary rocks (mainly conglomerates, sandstones, marls and claystone). Cambrian intrusive rocks (mainly granite and syenite) are also included (Whiteman, 1971).

The basement complex is overlain by the Mesozoic sedimentary sequences, mainly represented by the Nubian Sandstone Formation (mainly sandstones of Lower to Upper Cretaceous age) and locally by Cenozoic volcanic rocks (mainly basalts). Paleogene limestone are among the sole carbonatic rocks and outcrops only in north-western Sudan. Extensive Quaternary deposits, formed by gravel, sand and clayey materials, cover large areas not only near the river system. Quaternary sediments include sand dunes and sheets, and deposits formed in fluvial and lake environments; the latter are related to environmental conditions wetter than today. Going into detail, the White Nile and its catchments in the Sudanese territory (after the swamps of the Sudd, northern of Sud Sudan) insist on rocks of the basement complex (Whiteman 1971; Stern et al. 2006; Abdersalam and Stern 1996), locally intruded by Precambrian and Cambrian granitoids, and near to the confluence with the Blue Nile on the Mesozoic sedimentary sequences (Fig. 1). The Blue Nile pass through the Cenozoic volcanic rocks of the Ethiopian plateau and the Precambrian basement and the Mesozoic sedimentary sequences (Fig. 1), analogously also to the Atbara River. The Main Nile flows on terrains of the Precambrian basement complex and of the Mesozoic sedimentary sequences, locally intruded by Precambrian and Cambrian granitoids, especially near the VI, V, IV, III and II cataracts (Fig. 1).

Due to different solid load of each part of the river and its catchments, the composition of the sediments locally laid down will reflect not only the geology of the terrain that the river crossed, but also the contribution of its tributaries (Garzanti et al. 2015 and citations therein), especially for the Main Nile.

3. Materials and methods

Clayey materials have been sampled from the riverbanks along the Blue Nile (BN), White Nile (WN) and Main Nile after the confluence between White and Blue Nile in Khartoum (MN1) and after

that of the Atbara River (MN2). Preferential sampling points were located in the vicinity of attested Mesolithic, Neolithic and/or Meroitic archaeological sites (Figure 1). Bulk samples were collected from exposed outcrops along the present-day riverbanks at variable depth according to the local topography and after cleaning the outcrops' surface. In one case, samples were collected at different depth by hand-coring the plain in the vicinity of the Al Khiday prehistoric archaeological sites (clayey sediments 1, 1-35cm, 1-70cm, 1-90cm).

Samples have been studied adopting a multidisciplinary approach, consisting in petrographic analysis at the polarized light optical microscope (OM) and scanning electron microscope (SEM), mineralogical analysis by X-ray powder diffraction (XRPD) and thermal analysis (TA), bulk geochemical analysis by X-ray fluorescence (XRF), and Sr isotope analysis by Thermal Ionization Mass Spectrometry (TIMS).

More in detail, in order to obtain thin sections, the loose materials were mixed with ultrapure water in a plastic paste to prepare green briquettes, which were then air-dried for some days and fired at 500°C for 7 hours to remove the organic matter and be hardened. Thin sections, representing an analogous to ceramic material, were then analyzed under polarizing light microscope, with the description protocol reported by Whitbread (1986, 1989, 1995) and revised according to Quinn (2013).

Polished thin sections of the clayey sediments were also analyzed by SEM to detect the presence of possible mineralogical and petrographic markers, using a CamScan MX 2500 electron microscope, coupled with an energy dispersive spectrometer (EDS), equipped with a LaB_6 cathode, working in high vacuum mode (HV) and operating at 20 kV and 160 nA.

All the clayey samples were ground in an agate mortar and about 1 g of each sample was heated in a furnace at 860°C for ~ 20 minutes and then at 980°C for ~ 2 hours for the determination of loss on ignition (L.O.I.): the released volatile elements which can be identified as hydrogen, oxygen and carbon. Samples for XRF analysis were then prepared as glass beads mixing 0.65 g of calcined powder with di-lithium tetraborate $Li_2B_4O_7$ flux with a dilution ratio of 1:10 and melted using a fluxer Claisse Fluxy (~1150°C). XRF analysis were carried out using a WDS sequential Philips PW2400 spectrometer, and the following major and minor chemical elements (expressed as oxides wt%), and trace elements (expressed as ppm) were analyzed: SiO_2, TiO_2, Al_2O_3, Fe_2O_3, MnO, MgO, CaO, Na_2O, K_2O and P_2O_5; Sc, V, Cr, Co, Ni, Cu, Zn, Ga, Rb, Sr, Y, Zr, Nb, Ba, La, Ce, Nd, Pb, Th and U. Internal instrumental precision is within 0.6% relative for major and minor elements, and within 3% relative for trace elements. Detection limits are within 0.01% for major elements Al_2O_3,

MgO and Na_2O, within 0.2% for SiO_2, within 0.005% for TiO_2, Fe_2O_3, MnO, CaO, K_2O and P_2O_5. Detection limits for trace elements are (in ppm): Sc = 5, V = 5, Cr = 6, Co = 3, Ni = 3, Cu = 3, Zn = 3, Ga = 5, Rb = 3, Sr = 3, Y = 3, Zr = 3, Nb = 3, Ba = 10, La = 10, Ce = 10, Nd = 10, Pb = 5, Th = 3, U = 3. A set of geological standards, analytically tested by the international scientific community (Govindaraju, 1994), was used for calibration; they were supplied by the following agencies: USGS (United States Geological Survey, Reston, USA), CRPG (Centre de Recherches Pétrographiques et Géochimiques, France), ANRT (Association Nationale de la Recherche Technique, Paris, France), GIT-IWG (Groupe International de Travail - International Working Group, France), RIAP (Research Institute of Applied Physics, Irkutsk, Russia), GSJ (Geological Survey of Japan, Japan), MINTEK (Council for Mineral Technology, South Africa) and WIHG (Wadia Institute of Himalayan Geology, India).

The chemical data were then statistically treated using both univariate and multivariate approach. The R Project for Statistical Computing was used to explore the compositional variation matrix, according to the method proposed by Buxeda i Garrigós (1999). Chemical data were then processed with standard statistical tools such as Principal Component Analysis (PCA) and cluster analysis (CA) on a subset of elements, excluding those with a low ratio between total variation (vt) and variance (τ.i). Raw data were transformed according to procedures designed by Vitali and Franklin (1986), Baxter (1999) and Buxeda i Garrigós (1999), by log-normal ratio transformation and the centered log-ratio transformation, therefore data were transformed to the base 10 logarithm and divided by the element showing the lowest value of variance (τ.i) in order to avoid misclassifications due to the different orders of magnitude and range of variation of the variables (Papageorgiou 2020).

XRPD analysis was carried out using a Philips X-Pert PRO diffractometer (PW3710 parafocusing geometry Bragg-Brentano diffractometer) equipped with a copper anode, sample spinner, a goniometer PW3050/60 (Theta/Theta) with a minimum step size 2Theta = 0.001° and a RTMS detector (X'Celerator). The analyses were conducted in the range 3–80° 2Theta using a step interval of 0.017° 2Theta, with a counting time of 100 s. The phase identification and semi-quantitative analyses were performed using the software package X'Pert HighScore Plus (3.0 version) with which the shape of multiple peaks was closely examined. Phase identification was gained by the comparison with the reference pattern databases PDF2 (ICDD), Panalytical-ICSD and COD (Crystallography Open Database). XRPD patterns were statistically treated by cluster analysis according to the procedure proposed by Piovesan et al. (2013) and Maritan et al. (2015).

The thermal behavior of all the clayey materials was investigated by simultaneous thermal analyses (STA) under controlled humidity conditions: TG (thermal gravimetric and calculated differential thermal gravimetric: DTG) and DSC (differential scanning calorimetry), to respectively define loss of components and endothermic and exothermic transformations. For these purposes, was used a NETZSCHSTA 449 F3 Jupiter coupled with a FTIR BRUKER Tensor 27 for the Evolved Gas Analysis (EGA) by a transfer line heated at 200°C. Samples were heated from 40°C to 1050°C, with a heating rate of 10°C/min in nitrogen atmosphere (flow rate 60 mL/min). Thermal measurements were coupled with Fourier-transformation Infrared spectroscopy (FTIR) of the gas derived from the phase decomposition (EGA), to better correlate functional groups of the released volatiles with specific mass loss. TG and DSC curves were acquired and after processed with the NETZSCH Proteus6.1 Software.

High precision measurements of $^{87}Sr/^{86}Sr$ isotope ratios were performed by Thermal Ionization Mass Spectrometry (TIMS), using a Micromass VG 54E single-collector mass spectrometer. Approximately 1g of clayey powder were heated at 750°C for 1 night in platinum crucibles. Then ~100mgs were dissolved in Savillex PFA teflon vials by repeated acid attacks (1:4 = HNO3 : HF; 6.2N HCl), and final dissolution in 2.5N HCl. After ion-exchange chromatography on column to separate strontium from rubidium (BioRad AG50W-x12 resin), strontium eluates were loaded as nitrate over degassed single tungsten filaments, after a drop of a solution of $TaCl_5$ used as an activator. The software used for the acquisition of the isotopic data was 'Analyst' (Version 2.20; Ludwig 1985). The measured values of the $^{87}Sr/^{86}Sr$ isotopic ratio were typically normalized to a $^{86}Sr/^{88}Sr$ value of 0.1194 (the value obtained by Nier 1938) by assuming that the isotopic fractionation in the residue occurred according to the exponential model of mass fractionation of Russel et al. (1978). Over the time-span in which the measurements were performed, repeated analysis of NIST SRM 987 gave the following weighted-average value: 0.7102595 +/- 0.0000080 (2σ, n = 4). To measure the concentration of strontium by isotope dilution mass spectrometry (ID-MS), appropriate aliquots of an ^{84}Sr-enriched spike solution obtained by a Sr carbonate from Oak Ridge National Laboratories (enrichment ~82%) was added to the samples. The isotopic composition of the spike solution was determined using the method of Cavazzini (2005), and the strontium concentration was calculated by repeated (n = 2) mixing of the solution with appropriate aliquots of NIST SRM 911 to minimize error magnification. Isotope dilution data-reduction software was SAMSPK (Cavazzini 2001). Precision of the ID-MS Sr concentration results was ~ 0.4%.

4. Results and discussion

4.1 Petrographic analysis

The petrographic analysis of the fired briquettes revealed high variability of the clayey materials due to the different mineral phases and rock fragments occurring as inclusions (grains larger than 10 μm), both in terms of type, absolute and relative quantity, related to the geology of the associated hydrographic basins.

Clayey samples from the White Nile (WN) basin are all characterized by homogeneous groundmass, with inclusions composed of rounded to well-rounded quartz grains, associated to rare crystals of plagioclase, K-feldspar, white mica and biotite flakes, very rare crystals of amphibole, ilmenite and small carbonate inclusions (also caliche) and ochers (Fig. 2a-d). According to the sampling point they display different quantities of inclusions. More in detail, samples collected near Ed Dueim (clayey sediment 30 and 31) about 200 km south of the confluence with the Blue Nile, show poorly-sorted inclusions, up to 300 μm and 800 μm size respectively, with a c:f (coarse:fine) ratio of 30:70 (Fig. 2a-b). Samples collected near the Blue Nile confluence contain in one case (clayey sediment 1) well-sorted inclusions, up to 200 μm in size, with low c:f ratio (20:80) (Fig. 2c), whereas in the other (clayey sediment 2) more abundant (c:f ratio = 50:50) and larger-size inclusions with an average diameter of about 400 μm (Fig. 2d). The mineral-petrographic nature of inclusions in these clayey materials of the White Nile clearly reflect the geology of the hydrographic basin after the Sudd marshes, dominated by the metamorphic (high-grade gneiss and migmatites) and the granitoid rocks constituting the Precambrian basement, and the quartz-rich Nubian Sandstone. This is consistent with what observed by Garzanti et al. (2006, 2015) analyzing the petrography of sand-sized grains heavy minerals.

Clayey samples from the Blue Nile (BN) show different microscopic features, since abundant quartz grains are associated to alkali feldspar, plagioclase, subordinated amphibole, pyroxene, volcanic rock fragments often very weathered, biotite and white mica flakes (Fig. 2e-f). The clayey sediments collected from the eastern bank are characterized by well-sorted, fine-sand and silt sized inclusions (up to 100 μm), with a c:f ratio of 25:75 (clayey sediment 13, Fig. 2e), whereas those from the western bank that can be considered as part of the Gezira mega-alluvial fan (Fig. 1) (see Williams et al. 2000; Sulieman et al. 2016; Zerboni et al. in press) are poorly-sorted, with

inclusions up to 600 μm, sub-rounded in shape and with c:f ratio of 30:70 (clayey sediment 15, Fig. 2f). As suggested by Garzanti et al. (2006, 2015), the higher mafic component of the Blue Nile clayey sediments is consistent with the river headwater that is located along geology of the Ethiopian highlands. Therein the bedrock consists of volcanic and volcanoclastic rocks (mainly basalts and ignimbrites), across which the Blue Nile and its main tributary (Abay River) flow.

The clayey sediments collected along the banks of the Main Nile 1 (MN1) after the confluence between the White and the Blue Nile and before that of Atbara are characterized by low quantity of inclusions (e.g. c:f = 5:95 in sample 4 and 15:85 in sample 6B) with fine maximum grain-size (e.g. up to fine 40 μm in sample 4 and to 200 μm in sample 6B). They are composed of quartz, biotite and white mica, opaque minerals, K-feldspar (microcline), plagioclase, clinopyroxene, amphibole, volcanic rock fragments, weathered olivine, rare limestone fragments, and aggregates of montmorillonite (Fig. 3a-c). The latter represent the alteration products of volcanic mafic rocks, and forms fine silty-sized aggregates of lamellar crystals (Fig. 3c), similar to those also observed in the sediments from the Blue Nile.

Higher amount of mafic constituents are present also in the clayey material collected from the Atbara River (sample 9), characterized by a high c:f ratio (60:40) and inclusions reaching 150 μm. In this clayey sediment, inclusions includes sub-rounded quartz grains, abundant crystals of plagioclase, flakes of biotite, chlorite and subordinated white mica, crystals of clinopyroxene, olivine, weathered volcanic rock fragments and opaque minerals (Fig. 3d). As for the Blue Nile, Atbara's sediments reflect the composition of the Cenozoic volcanic rocks of its catchment and of its occasional affluents, as the Gash River (Fig. 1) (Costanzo et al., 2021).

Very similar to the Atbara clayey sediments is also the sample collected along the Main Nile 2 (MN2) after their confluence (sample 8), in both textural and composition terms (high c:f ratio and mineral-petrographic nature of inclusions) (Fig. 4a). But when the distance from the confluence between the Atbara and the Main Nile increases, the quantity of mafic minerals decreases, since the sandy heavy fraction undergoes progressive deposited, being depleted from the transported silty and sand-sized fragments. Clayey materials collected after the IV cataract are composed by abundant quartz, subordinated crystals of K-feldspar, plagioclase, fragment of volcanic mafic rocks, flakes of white mica and biotite, scarce pyroxene, amphibole, opaque minerals and carbonate rocks fragments (Fig. 4b-c). From a textural point of view these clayey materials are quite similar (e.g. 21 and 28), with c:f ratio = 15:85, grain-size up to 200 μm (Fig. 4b-c). Finally, the clayey materials collected between the III and the II cataract (e.g. 24) are characterized by fewer

inclusions, up to 100 μm in size, formed by predominant quartz, subordinated microcline, plagioclase, opaque minerals and rare pyroxene and white mica (Fig. 4d).

It is important to remark that the clayey sediments collected along the Nile river in Sudan display textural features (in terms of abundance of silt and sand fractions), which depends on the local hydrodynamic conditions and sedimentary facies. But the nature of the inclusions clearly indicates important differences among the various segments of the river (WN, BN, MN1, MN2) which ultimately depend on the geology of the headwaters and catchments. Garzanti et al. (2006, 2015) and Padoan et al. (2011) found general trends differing along each segment of the Nile River based on the petrography of sands, and the inter-sample compositional variability was interpreted in terms of their grain size.

4.2 Mineralogical composition

The mineralogical analysis by XRPD data indicates that the clayey materials contain, in different proportions, quartz, plagioclase, K-feldspar, calcite, amphibole, pyroxene, montmorillonite, illite/muscovite and kaolinite, according to the related hydrographic catchment. Since the quantification of mineral phases in such a complex type of polyphase geomaterials (mainly characterized by the occurrence of clay minerals which tend to orient parallel to the (00l)), is bases on a procedure time consuming and expensive, in the present study a different approach, based on the statistical comparison between pattern profiles, was adopted to emphasize the differences between samples. When statistically treated by cluster analysis (according to Piovesan et al. 2013, and Maritan et al. 2015), XRPD data tend to cluster according to position and intensity of diffraction peaks (Fig. 5). The dendrogram obtained from the cluster analysis (Fig. 5) indicates that the clay materials from the White Nile and those from the Gezira mega-fan are grouped in adjacent clusters (CL1-CL4), whereas those from the Main Nile 1 cluster all together with some of the Main Nile 2 (just after the confluence with the Atbara) in cluster CL5, those from the Blue Nile in cluster CL6 and those of the Main Nile 2 in cluster CL7 and CL8. Three outliers are represented by the clayey sediments from the Atbara (9), and two from the Main Nile (4 and 20). Going into more detail, clay materials collected near Ed Dueim along the White Nile (30 and 31), before the Gezira plain (corresponding to a mega-fan, therefore defined as the Gezira Fan; see Williams et al. (2015)), clearly differ from all the others for the high dissimilarity level, since they are very rich in quartz and contain subordinate plagioclase, calcite, kaolinite and very little montmorillonite (Fig. 6a). Moving northwards along the White Nile, a second cluster (CL2) comprises clayey materials

collected from the Pleistocene lake sediments (Williams et al., 2015; Spinapolice et al., 2018) and on the left bank of the White Nile just after the Jebel Aulia dam (where little sediment of the river is nowadays deposited), characterized by a higher content of quartz, associated to very low quantity of plagioclase, calcite and kaolinite. Microscopic evidence of quartz-rich lake sediments reported in Zerboni (2011) and Williams et al. (2015) supports our data. Clayey materials collected from the Gezira Plain, reflect the mixing of the White and Blue Nile deposits, despite those sampled near the Blue Nile contain more calcite (Fig. 6c), which is likely inherited by the dismantling of pedogenic carbonates (samples 15 and 16 are soils collected in the plain far from the river banks) that are very common in the region (Dal Sasso et al., 2018; McCool, 2019), while those from the White Nile are richer in kaolinite and contain illite/muscovite (Fig. 6d), a character also described by Garzanti et al. (2015). Clayey sediments of the Blue Nile (cluster CL6) are characterized by a high content of montmorillonite, associated to illite/muscovite and kaolinite as clay minerals, in addition to quartz, plagioclase, feldspar, calcite, pyroxene and amphibole (Fig. 6h). Analogous mineralogical association is attested also for the clayey material of the river Atbara River, although characterized by lower quantity of calcite and higher content in pyroxene (Fig. 6e). As for the Main Nile, all the samples show high content in montmorillonite, associated to illite/muscovite and kaolinite, as well as high content in plagioclase, and often in amphibole and pyroxene (Fig. 6g, i, l), consistently with the clayey sediments of the Blue Nile and Atbara, from which they receive the greater solid contribution (Garzanti et al., 2015 and citations therein). A peculiar case is represented by the clayey materials collected just before the VI cataract and after the IV cataract (4 and 20, respectively) (Fig. 6f), where granite and syenite complexes outcrop. For this reason, these materials show higher kaolinite (from the weathering of the feldspars) and calcite contents and lower quartz.

It is important, therefore, to remark that clayey materials studied in this research are affected, in compositional terms, by the proportions between clay minerals (sheet silicates) and aplastic fragments (lithic and mineral) mainly constituting the silty and sandy fractions of the collected sediments. Therefore, possible differences in quantitative terms with the mineralogical composition of sediments of the Nile system as reported by Garzanti et al. (2015) can be explained considering the dilution effect caused by the sand-sized fraction.

The presence of clay minerals of the smectite group (montmorillonite) in the clayey materials here studied is also confirmed by the weight loss in the thermal interval between 100°C and 200°C and the occurrence of an endothermic peak around 150°C (see DSC data in Table 3) related to the loss

384 of interlayer water, as shown by FTIR-EGA. This characteristic peak is observed in clayey materials
385 from the Blue Nile, Atbara, Main Nile (MN1 and MN2) and those collected from the Gezira Plain
386 (White Nile right bank), whereas those collected from the White Nile and from the Pleistocene to
387 Holocene wetland deposits (Williams et al., 2006, 2015; Cremaschi et al., 2007; Williams and
388 Jacobsen, 2011; Zerboni, 2011) do not contain smectite minerals. Since the clay sediments contain
389 different quantity of clay minerals and other phases, as well as different proportions between the
390 various clay minerals (illite, smectite, kaolinite, chlorite), in order to better define the content of
391 smectite, the quantity of interlayer water (weight loss between 100 and 200°C) was divided by the
392 total weight loss due to the clay minerals (summing the weight loss of the thermal interval 100-
393 200°C, 400-600°C and 850-1050°C) (Fig. 7a). This approach was preferred to the quantification
394 based on XRPD data, since the quantitative analysis by Rietveld method (normally used) of clay
395 minerals can suffer of great errors due to preferential orientation of the clay mineral flakes, as
396 well as the presence of many other mineral phases for which the structural model is difficult to
397 choose for the intrinsic nature of the sedimentary deposits (such as the occurrence of various
398 terms of isomorphic minerals). Although the different minerals of the smectite group have
399 different water content, diffraction patterns of the analyzed clays, as well as the chemical
400 composition determined by microanalysis at the SEM on the aggregates observed in thin section,
401 indicate that it is invariably montmorillonite.
402 The thermal analysis of the clayey sediments also allowed to define the content of organic matter
403 and calcite. More in detail, organic matter was determined by the weight loss in the thermal
404 interval 200-400°C (Table 2) and resulted to vary between 0.7% to 3.5% but without any
405 systematic trend for the various river branches (Fig. 7b). Calcite content was determined using the
406 CO_2 released in the thermal interval 600-850°C and resulted to range mostly between 1 and 4%
407 (Fig. 7c) with the exception of clayey sediment 16, which resulted to have 5.7% of calcite. This
408 sample was collected along the Gezira Plain, quite far from the Nile banks, where soils are
409 occasionally enriched in calcium carbonate nodules and concretions (Buursink, 1971). It might be
410 argued that in the case of sample 16 the occurrence of calcite is relate to the precipitation of soil
411 carbonates.
412
413 **4.3 Geochemical composition**
414 When the geochemical composition is considered, an interesting picture arises. All the samples
415 from the White Nile, also those collected from the eastern river bank along the Gezira Plain (WN-

G) and those from the area of the Upper Pleistocene and Holocene wetlands (WN-L), cluster together (Cluster 1 in Fig. 7a). Only one sample from the Main Nile 1 (4), collected immediately downstream the outcrops of granite and syenite, resulted to be geochemically very similar to the White Nile sediments (Figure 7a), and in particular to those from the Gezira Plain. This is related to the contribution of sediments derived from the weathering of acidic rocks and transported towards the Nile from the east by a network of local wadis, causing a dilution effect on the more mafic composition characteristic of the Blue Nile and therefore also of the Main Nile. Clayey materials from the Gezira Plain collected near the Blue Nile (BN-G) form a separate group (Cluster 2 in Fig. 7a), which shows higher similarity with samples from the White Nile than from the Main Nile and Atbara, being more dissimilar from the latter. This geochemical affinity reflects the mixing between the sediments of the two Niles (WN + BN) in the Gezira Plain, with different proportion than the sediments of the Main Nile after their confluence. All the samples from the Main Nile 1 (MN-1) cluster together, along with some of the Main Nile 2 (MN-2) and that of the Blue Nile (BN) (Cluster 3 in Fig. 8a), whereas the clayey sediment of river Atbara resulted to be isolated.

Geochemical grouping can be better interpreted on the basis of the principal component analysis (PCA), which allows to define the chemical variables responsible for the variance among samples. According to the score and loading plots of the PCA (Fig. 8b, c), clayey sediments from the White Nile are generally richer in silica, potassium and some trace elements, such as zirconium, thorium, uranium, cerium and rubidium. Clayey sediment of the Atbara is richer magnesium, calcium, sodium, strontium and chromium, reflecting the origin of its sediments from the Cenozoic basalts. Clayey materials from the Main Nile and Blue Nile overlap within a large group. Only part of the Main Nile sediments after the confluence with the Atbara (MN-2) show negative values of PC2, reflecting higher concentration in iron, aluminum, manganese, zinc, lead and cobalt, whereas those of the Main Nile before the Atbara confluence (MN-1) are poorer in these elements. Clayey materials from the Gezira Plain are plotted between the White Nile and the Main Nile-Blue Nile distribution clouds, being those collected near the White Nile banks (WN-G) poorer in calcium, and richer in aluminum, silica, titanium and iron, therefore richer in clay minerals than those collected further west near the Blue Nile (BN-G).

Focusing on the core samples collected along the White Nile (clayey sediments 1, 1-35, 1-70, 1-90), their chemical variability is expressed by the wide range of the PC2, which is mainly related to the aluminum content, thus suggesting that the chemical variability is mainly controlled by the abundance of clay minerals.

448 The geochemical differences among the various catchments of the Nile system, although
449 differently expressed, can be also observed in the element concentration standardized to the
450 upper continental crust for the mud fraction as published by Garzanti et al. (2015). They are
451 related to the geological nature of the terrains on which the various branches of the Nile systems
452 and its tributaries flow. The geochemical features of the White Nile sediments in Sudan after the
453 Sudd marshes (northern South Sudan), where most of the sediment load from the Uganda,
454 Rwanda and Burundi is retained, are consistent with an origin from the high-grade metamorphic
455 rocks (gneiss and migmatites) and granitoids of the Precambrian basement, and from the
456 Mesozoic sedimentary sequences of the Arabian-Nubian Shield, mainly presented by the Nubian
457 Sandstone Formation (Whiteman, 1971; Stern et al., 2006; Abdersalam and Stern, 1996) (Fig. 1).
458 The Blue Nile, and its main tributary Abay River, as well as the Atbara River, originate from the
459 Ethiopian plateau formed by Cenozoic volcanic rocks (alkaline and tholeiitic basalts and
460 ignimbrites), and then cross the Precambrian basement and the Mesozoic sedimentary sequences
461 (Fig. 1). Therefore, the clayey materials of the Blue Nile, Atbara and consequently of the Main Nile,
462 in one word the sediment load of which is mainly due to the Blue Nile contribution (Garzanti et al.,
463 2015 and citations therein), result to be more mafic in composition.
464 As concerns strontium isotope composition (Table 1), clay materials collected along the White Nile
465 are characterized by higher $^{87}Sr/^{86}Sr$ values (0.709396 - 0.712120), congruently with their origin
466 from the Precambrian basement and the Nubian Sandstone Formation (which comprises the
467 sedimentary sequences from the Paleozoic to the Cenozoic)(Fig. 9a, b), whereas those collected
468 along the Blue Nile River are characterized by lower $^{87}Sr/^{86}Sr$ values (0.705781 - 0.707070)
469 reflecting the initial isotopic signature and the low Rb/Sr ratio of the parental volcanic basic rocks.
470 This also occurs for samples collected along the Main Nile after the confluence with Atbara River
471 (MN-2). This affinity resides in the contribution in terms of sediment load derived from both Blue
472 Nile and Atbara River that are responsible for more than 90% to the total sediment budget of the
473 Main Nile (Woodward, 2007; Padoan et al., 2011; Garzanti et al., 2015). This is due also to higher
474 strontium contents in the basic rocks with respect to significantly lower strontium contents in the
475 rocks of the crystalline basement. Clayey sediments derived from the Gezira Plain (WN-G and BN-
476 G) show lower $^{87}Sr/^{86}Sr$ values (0.707857 - 0.708218), that seem to be a mix of White Nile and Blue
477 Nile $^{87}Sr/^{86}Sr$ values (Fig. 9a-d).
478 As regards the core-drill specimens collected along the White Nile near the Al Khiday site, clayey
479 sediment 1-90 as well as the other samples (1-70 and 1-35) show strontium isotopic ratio higher

than clayey sediment 1 that was collected in the same location, but from the surface (Table 2). This is probably due to a superficial mixing of the sediments related to a high flood episode of the Blue Nile occurred a few decades ago, or to the mixing with recent wind-blown sediments. Moreover, the core-drill samples are probably more ancient than clay 1 and reflect the situation before the construction of the Jebel Aulia dam in 1937, located 35 km south of Khartoum. At that time, sediments of the White Nile were not impeded by any barrier and the crustal fingerprint deriving from the dismantling of the crystalline basement was more evident downstream. Some ambiguities regard also clayey sediment 30, collected at Ed Dueim, 200 km south of Al Khiday along the White Nile. It shows a lower Sr isotopic ratio than that of the White Nile clayey sediments from Al Khiday, even if it is located away from the Blue Nile course (Table 2). Although clayey sediment 30 was collected along the eastern bank of the White Nile, *i.e* at the edge of the Gezira Plain, it still shows the influence of the Blue Nile. In fact, 14,500 years ago the White Nile deposited clayey sediments along its flood plain and simultaneously reworked pre-existing sand and gravel brought in by the late Pleistocene Blue Nile channels that flowed across the Gezira mega-fan (Williams et al. 2015). Thus, the present-day clayey material collected at Ed Dueim most likely still shows the $^{87}Sr/^{86}Sr$ value of the reworked mixed sediments located along the eastern bank of the White Nile.

The composition of systems which represent mixtures of two end-members in variable proportions can be expressed in terms of two or more measured variables, such as isotope ratios, elemental ratios, and elemental abundances (Faure and Powell, 1972; Faure, 1977; Faure and Mensing, 2005; Dickin, 2006). In this context, the behavior of $^{87}Sr/^{86}Sr$ isotopic tracers was considered as a function of Sr concentration (Fig. 9b). Ideally, initial Sr isotope ratios should be plotted against the abundance of ^{86}Sr but, since the half-life of Rb is low (48–49 billion years), ^{88}Sr makes up the bulk of strontium in most rocks and the abundance of ^{86}Sr can be approximated by total Sr without introducing significant errors (Faure, 1977; Dickin, 2006). Mixing of two components with different isotopic and elemental compositions produces a hyperbolic curve on a diagram of $^{87}Sr/^{86}Sr$ ratio against Sr concentration (Fig. 9b), if are excluded the two samples of the White Nile and the Pleistocene lakes (sample 2 and 11, respectively). These samples are rich in sand and characterized also under a geochemical viewpoint by high silica concentration and much lower strontium content (for the dilution effect of quartz, which is a Sr-free mineral). However, strontium isotope ratios of those samples are consistent with the area of origin. When $^{87}Sr/^{86}Sr$ values are plotted against 1/Sr (approximating $1/^{86}Sr$) (Fig. 9c), a straight line describes the mixing

between the two end-members: Sr concentration increases as Sr isotope ratio decreases progressively from clayey materials draining crystalline basement products (White Nile) to clayey sediments deriving from Ethiopian plateau (Blue Nile and Atbara River). The three samples with the highest $^{87}Sr/^{86}Sr$ value derive from the core drilled underneath clayey sediment 1 and they show the typical crustal signature of the crystalline basement and sedimentary clastic sequence derived from its disruption.

These isotopic results only partially match those obtained by Padoan et al. (2011) and Garzanti et al. (2015). The reason for this is that the authors analyzed the silt (> 40-63 μm) and the sand (63-2000 μm) fractions separately, and they reported the results as a mean of a series of measures, losing any detail concerning the analysis of the segments of the Sudanese Nile basin, since they considered the whole Nile River from its springs to the delta (Fig. 9d). In particular, the $^{87}Sr/^{86}Sr$ values of White Nile, Main Nile 1 (MN-1), Main Nile 2 (MN-2) and Blue Nile (BN) respectively match the values obtained in this study, but the Sr content shows variability, reflecting the analysed grain-size fractions, with sand having lower Sr values for the White Nile and higher ones for the Main Nile than the respective fine fractions obtained by sieving from the levees.

These data are quite important because they indicate that Sr isotope ratio is barely affected by the grain-size, within certain limits.

5. Conclusions: implication on pottery provenance and human mobility

The multi analytical analysis of the clayey materials collected along the Nile system in Sudan provided a reference database to be used for archaeometric analysis of ancient pottery productions and provenance, and consequently for studying ancient individual mobility of the communities living close to the Nile River banks. In fact, traditional investigation on pottery composition can in some cases not be able to discriminate on the origin of raw materials. For instance, the high abundance of quartz in many of the ancient pottery production of this region (see Dal Sasso et al., 2014 and citations therein) and the lack of other petrographic markers hamper the possibility to reconstruct human mobility and trade network in ancient times if only geological maps are considered. Yet, an integrate analysis that comprised petrographic, mineralogical, chemical and isotopic approaches can efficiently discriminate the ancient production areas of pottery, thus highlighting what archaeological materials have moved or exchanged along the Nile in ancient times.

The microscopic petrographic and microstructural analyses allowed to define the occurrence of large sub-rounded to rounded quartz grains resulted to be more characteristic of the clayey samples collected along the White Nile, whereas that of small angular and sub-angular quartz grains is typical of sediments from the catchments originating from the Ethiopian Highlands. Furthermore, the occurrence of other phases such as plagioclase, olivine and pyroxene, contributed to characterize the volcanic origin of these sediments, as well as the SEM analysis highlighted the presence of montmorillonite-rich aggregates derived from the weathering of basaltic rocks. These phases were found only in clayey sediments collected along the Blue Nile and the Main Nile and might be considered as diagnostic for the discrimination of the raw materials used in ancient ceramic productions.

As regards the mineralogical analysis, the statistical treatment of data revealed a good clustering of samples collected along the main tributaries (White Nile, Blue Nile, Atbara) but partially failed in discriminating clayey sediments obtained from the main branch of the Nile River (Main Nile 1 and Main Nile 2), since the mineral composition of the Main Nile after the confluence of the two rivers is strongly affected by the contribution of Blue Nile. Some exceptions were explained by the influence of sediments brought from inactive tributaries of the Nile, the remixing of which still affects the mineralogical and chemical composition of the clay materials.

Based on the chemical composition of the clayey sediments, some discrimination among the different sectors of the river Nile is possible, but strontium isotope ratio better point out the mixing processes involving the sediments of the Nile River. White Nile clayey sediments have a high $^{87}Sr/^{86}Sr$ ratio, with the highest values for samples from core-drill, probably reflecting the stronger contribution of the White Nile before the construction of the Jebel Aulia dam, and the lowest value for those collected at the surface, influenced by a recent episodic flood event of the Blue Nile. Clayey materials form the Gezira Plain are influenced by the presence of the Blue Nile. For over a century the Blue Nile overflowed, thus stemming the White Nile through a network of distributary channels that flowed across the Gezira mega-fan (Williams et al. 2015). Clayey sediments collected along the Blue Nile show $^{87}Sr/^{86}Sr$ values comparable with those of the Main Nile, indicating that Nile River maintains a mixed fingerprint.

Strontium isotopic data provided important complementary constraints to assess clayey sediments provenance in addition to bulk geochemistry, thus representing a potentially useful tool also to constrain the provenance of ancient pottery, especially when petrographic markers are

scarce or absent due to the dilution effect of a quartz-sand temper, as it is often the case in the Sahara and Sub-Saharan productions.

Credit author statement

Lara Maritan, Claudio Mazzoli, Sandro Salvatori, Donatella Usai, Andrea Zerboni, Abdelrahman Ali Mohamed: Conceptualization; Giancarlo Cavazzini, Elisa Gravagna, Lara Maritan, Mariano Mercurio, Celestino Grifa: Data curation; Elisa Gravagna, Giancarlo Cavazzini, Lara Maritan, Mariano Mercurio, Celestino Grifa: Formal analysis; Lara Maritan: Funding acquisition; Lara Maritan, Elisa Gravagna, Giancarlo Cavazzini, Andrea Zerboni, Mariano Mercurio, Celestino Grifa: Investigation; Giancarlo Cavazzini, Elisa Gravagna, Lara Maritan, Mariano Mercurio, Celestino Grifa: Methodology; Lara Maritan, Donatella Usai, Abdelrahman Ali Mohamed: Project administration; Lara Maritan, Sandro Salvatori, Donatella Usai: Supervision; Giancarlo Cavazzini, Elisa Gravagna, Lara Maritan, Mariano Mercurio, Celestino Grifa: Validation; Lara Maritan, Elisa Gravagna, Giancarlo Cavazzini, Andrea Zerboni, Donatella Usai: Visualization; All the authors: Roles/Writing - original draft; All the authors: Writing - review & editing.

Acknowledgements

The authors would like to thank Dr. Abdelhai Abdelsawy and Mongeda Khaleb Magzoub of the National Corporation for Antiquities and Museum (Khartoum, Sudan) and Ahmed Al Turabi of Sharka Tumbus llsiaha Al Mahduda for supporting logistics during the clay materials sampling. A special thanks to Gian Luca Zacchiroli for the photographic support during the field campaigns. This research is part of the activities promoted by the Centro Studi Sudanesi e Subsahariani (CSS&S) and supported by the Italian Ministry of Foreign Affair.

Funding: this work was supported by the University of Padova, within the project “Isotope analysis for pottery provenance studies” [grant number: BIRD160990/16].

605 **References**

606

607 Adamson, D., Williams, F., 1980. Structural geology, tectonics and the control of drainage in the
608 Nile basin. In: M.A.J. Williams and H. Faure (eds.), The Sahara and the Nile. Balkema, Rotterdam,
609 pp. 225-252.

610

611 Alex, B.A., Nichols, D.L., Glascock, M.D., 2012. Complementary compositional analysis of formative
612 period ceramics from the Teotihuacan Valley. Archaeometry 54, 821-834.

613

614 Baxter, M.J, 1999. Detecting multivariate outliers in artefact compositional data. Archaeometry 41,
615 321-338.

616

617 Budja, M., 2006. The transition to farming and the ceramic trajectories in Western Eurasia: from
618 ceramic figurines to vessels. Documenta Praehistorica 33, 183-201.

619

620 Buursink, J., 1971. Soils of the central Sudan. Published doctoral thesis, Utrecht University, The
621 Netherlands.

622

623 Buxeda i Garrigós, J., 1999. Alteration and Contamination of Archaeological Ceramics: The
624 Perturbation Problem, Journal of Archaeological Science 26, 295-313.

625

626 Carter, S.W., Wiegand, B., Mahood, G.A., Dudas, F.O., Wooden, J.L., Sullivan, A.P., Bowring, S.A.,
627 2011. Strontium isotopic evidence for prehistoric transport of Gray-Ware ceramic materials in the
628 eastern Grand Canyon region, USA. Geoarchaeology: An International Journal 26, 189-218.

629

630 Cavazzini, G., 2001. Samspk. Programma per convertire il rapport Sam/Spk fornito dal programma
631 'Analyst' di K.R. Ludwig (Berkeley Geochronology Center) in valori di concentrazione. Internal
632 report n. 61, Centro di Studio per la Geodinamica Alpina.

633

634 Cavazzini, G., 2005. A method for determining isotopic composition of elements by thermal
635 ionization source mass spectrometry: Application to strontium. International Journal of Mass
636 Spectrometry 240(1), 17-26.

637

638 Costanzo, S., Zerboni, A., Cremaschi, M., Manzo, A., 2021. Geomorphology and (palaeo-)
639 hydrography of the Southern Atbai Plain and western Eritrean Highlands (Eastern Sudan/Western
640 Eritrea). Journal of Maps. Journal of Maps 17, 51-62.
641

642 Cremaschi, M., Salvatori, S., Usai, D., Zerboni, A., 2007. A Further “tessera” to the Huge “mosaic”:
643 Studying the Ancient Settlement Patterns of the El Salha Region (South-west of Omdurman,
644 Central Sudan). Archaeology of Early Northeastern Africa, (eds.) Kroeper K, Chłodnicki M,
645 Kobusiewicz M, Poznań Archaeological Museum, Berlin, pp. 39-48.
646

647 Dal Sasso, G., Zerboni, A., Maritan, L., Angelini, I., Compostella, C., Usai, D., Artioli, A., 2018.
648 Radiocarbon dating reveals the timing of formation and development of pedogenic calcium
649 carbonate concretions in Central Sudan during the Holocene. Geochimica et Cosmochimica Acta
650 238, 16-35.
651

652 De Bonis, A., Arienzo, I., D'Antonio, M., Franciosi, L., Germinario, C., Grifa, C., Guarino, V., Langella,
653 A., Morra, V., 2018. Sr-Nd isotopic fingerprinting as a tool for ceramic provenance: its application
654 on raw mate- rials, ceramic replicas and ancient pottery. Journal of Archaeological Science 94, 51-
655 59.
656

657 Eramo, G., 2020. Ceramic technology. How to recognize clay processing. Archaeological and
658 Anthropological Sciences 12, 164.
659

660 Faure, G., 1977. Principles of Isotope Geology. John Wiley and Sons, New York.
661

662 Faure, G., Mensing, T.M., 2005. Isotopes: Principles and Applications. John Wiley & Sons, New
663 York.
664

665 Faure, G., Powell, J.L., 1972. Strontium isotope geology, Springer-Verlag, New York.
666

667 Garzanti, E., Andò, S., Vezzoli, G., Abdel Megid, A.A., El Kammar, A., 2006. Petrology of the Nile
668 River sands (Ethiopian and Sudan): sediment budgets and erosion patterns. Earth and Planetary
669 Science Letters 258, 327-341.
670
671 Garzanti, E., Andò, S., Padoan, M., Vezzoli, G., El Kammar, A., 2015. The modern Nile sediment
672 system: processes and products. Quaternary Science Reviews 130, 9-56.
673
674 Garzanti, E., Padoan, M., Setti, M., Lopez-Galindo, A., Villa, I.M., 2014. Provenance versus
675 weathering control on the composition of tropical river mud (southern Africa). Chemical Geology
676 366, 61-74.
677
678 Gliozzo, E., 2020. Ceramics investigation. Research questions and sampling criteria. Archaeological
679 and Anthropological Sciences 12, 202.
680
681 Govindaraju, K., 1994. Compilation of working values and sample description for 383
682 geostandards. Geostand. Newslett. 18, 1-158.
683
684 Hein, A., Kilikoglou, V., 2020. Ceramic raw materials. How to recognize them and locate the supply
685 basins Chemistry. Archaeological and Anthropological Sciences 12, 180.
686
687 Hommel, P., Day, P.M., Jordan, P., Vetrov, V.M., 2016. Context is Everything: Early Pottery, Hunter-
688 gatherers and the Interpretation of Technological Choices in Eastern Siberia. In E. Sibbesson, B.
689 Jervis, and S. Coxon (eds.), Insight from Innovation: New Light on Archaeological Ceramics. Papers
690 in Honour of Professor David Peacock. Southampton Monographs, Southampton, pp.1-18.
691
692 Honegger, M., 2014. Recent Advances in Our Understanding of Prehistory in Northern Sudan. In
693 J.R. Anderson and D.A Welsby (eds), *The Fourth Cataract and beyond. Proceedings of the 12th*
694 *International Conference of Nubian Studies*, Peeters Publishers, Leuven, pp. 19-30.
695
696 Huysecom, E., Rasse, M., Lespez, L., Neumann, K., Fahmy, A., Ballouche, A., Ozainne, S., Maggetti,
697 M., Tribolo, C., Soriano, S., 2009. The emergence of pottery in Africa during the tenth millennium
698 cal BC: new evidence from Ounjougou (Mali). Antiquity 83, 905-917.

699
700 Kibaroglu, M., Kozal, E., Klügel, A., Hartmann, G., Monien, P., 2019. New evidence on the
701 provenance of red lustrous wheel-made ware (RLW): petrographis, elemental and Sr-Nd isotope
702 analysis. Journal of Archaeological Science Reports 24, 412-433.
703
704 Jesse, F., 2010. Early pottery in Northern Africa. Journal of African Archaeology 8, 219-238.
705
706 Li, B.P., Zhao, J.X., Greig, A., Collerson, K.D., Feng, Y.X., Sun, X.M., Guo, M.S., Zhuo, Z.X., 2006.
707 Characterisation of Chinese Tang Sancai from Gongxian and Yaozhou kilns using ICP-MS trace
708 element and TIMS Sr-Nd isotopic analysis. Journal of Archaeological Science 33, 56-62.
709
710 Ludwig, K.R., 1985. Analyst (Version 2.20), User's manual for ANALYST; a Computer Program for
711 Control of an Isomass 54E Thermal-Ionization, Single-Collector Mass Spectrometer. USGS Open-
712 File Report 85-141.
713
714 Macklin, M.G., Toonen, W.H.J., Woodward, J.C., Williams, M.A.J., Flaux, C., Marriner, N., Nicoll K.,
715 Verstraeten, G., Spencer, N., Welsby, D., 2015. A new model of river dynamics, hydroclimatic
716 change and human settlement in the Nile Valley derived from meta-analysis of the Holocene
717 fluvial archive. Quaternary Science Reviews 130, 109-123.
718
719 Makarona, C., Mattielli, N., Laha, P., Terryn, H., Nys, K., Claeys, Ph., 2016. Leave no mudstone
720 unturned: geochemical proxies for provenancing mudstone temper sources in South-Western
721 Cyprus. Journal of Archaeological Science Reports 7, 458-464.
722
723 McCool, J.P., 2019. Carbonates as evidence for groundwater discharge to the Nile River during the
724 Late Pleistocene and Holocene. Geomorphology 331, 4-21.
725
726 Maritan, L., 2019. Archaeo-ceramic 2.0: investigating ancient ceramics using modern technological
727 approaches. Archaeological and Anthropological Sciences 11, 5085-5093.
728
729 Maritan, L., Holakooei, P., Mazzoli, C., 2015. Cluster analysis of XRPD data in ancient ceramics:
730 what for? Applied Clay Science 114, 540-549.

Maritan, L., Iacumin, P., Zerboni, A., Venturelli, G., Dal Sasso, G., Linseele, V., Talamo, S., Salvatori, S., Usai, D., 2018. Fish and salt: The successful recipe of White Nile Mesolithic hunter-gatherer-fishers, Journal of Archaeological Science 92, 48-62.

Ministry of Energy & Mining, Geological Research Authority of Sudan, 2004. Geological Map of the Sudan 1:2,000,000 scale.

Montana, G., 2020. Ceramic raw materials. How to recognize them and locate the supply basins. Archaeological and Anthropological Sciences 12, 175.

Nier, A.O., 1938. The isotopic constitution of strontium, barium, bismuth, thallium and mercury Physical Review 54, 275-278.

Out, W.A., Ryan, P., García-Granero, J.J., Barastegui ,J., Maritan, L., Madella, M., Usai, D., 2016. Plant exploitation in Neolithic Sudan: A review in the light of new data from the cemeteries R12 and Ghaba. Quaternary International 412, 36-53

Padoan, M., Garzanti, E., Harlavan, Y., Villa, I.M., 2011. Tracing Nile sediment sources by Sr and Nd isotope signature (Uganda, Ethiopia, Sudan). Geochimica et Cosmochimica Acta 75, 3627-3644.

Papageorgiou, I., 2020. Ceramic investigation. How to perform statistical analyses. Archaeological and Anthropological Sciences 12, 210.

Piovesan, R., Dalconi, C., Maritan, L., Mazzoli, C., 2013. X-ray powder diffraction diagram clustering and quantitative phase analysis on historic mortars. European Journal of Mineralogy 25, 165-175.

Quinn, P.S. 2013. Ceramic petrography: the interpretation of archaeological pottery and related artefacts in thin-sections. Archaeopress, Oxford.

761 Renson, V., Neff H., Martínez-Cortiza,s A., Blomster, J.P., Cheetham, D., Glascock, M.D., 2021. Lead
762 and strontium isotopes as tracers for Early Formative pottery exchange in ancient Mexico. Journal
763 of Archaeological Science 126, 105307.
764
765 Roosvelt, A.C., Lima da Costa, M., Lopes Machado, C., Michab, M., Mercier, N., Valladas, H.,
766 Feathers, J., Barnett, W., Imazio da Silveira, M., Henderson, A., Silva J., Chernoff, B., Reese, D.S.,
767 Holman, J.A., Toth, N., Schick, K., 1996. Paleo-Indian Cave Dwellers in Amazon: The Peopling of the
768 Americas. Science 272, 373-384.
769
770 Russell, W.A., Papanastassiou, D.A., Tombrello, T.A., 1978. Ca isotope fractionation on the Earth
771 and other solar system materials. Geochimica et Cosmochimica Acta 42, 1075-1090.
772
773 Said, R., 1981. The Geological Evolution of the River Nile. Springer-Verlag, New York.
774
775 Salvatori, S., Usai, D., 2019. The Mesolithic and Neolithic in Sudan. In: Raue, D., (Ed.), Handbook of
776 Ancient Nubia. De Gruyter, Germany, pp. 171-193.
777
778 Shelach, G., 2012. On the invention of pottery. Science 336, 1644-1645.
779
780 Shen, J.Y., Ma, H., Henderson, J., Evans, J., Chenery, S., Wang, F., Wen, R., 2019. Chemical and
781 strontium isotope analysis of Yaozhou celadon glaze. Archaeometry 61, 1039-1052.
782
783 Siam, M.S., Elthair, E.A.B., 2017. Climate change enhances interannual variability of the Nile river
784 flow. Nature Climate Change 7, 350–355.
785
786 Spinapolice, E.E., Zerboni, A., Meyer, M., Usai, D., 2018. Early human occupation at al-Jamrab
787 (White Nile region, central Sudan): a contribution to the understanding of the MSA of Eastern
788 Africa. Journal of African Archaeology 16, 193-209.
789
790 Sulieman, M.M., Ibrahim, I.S., Elfaki, J.T., 2016. Genesis and Classification of Some Soils of
791 the River Nile Terraces: A Case Study of Khartoum North, Sudan. Journal of Geoscience and
792 Environment Protection 4, 1-16.

Talbot ,M.R., Williams, M.A.J., 2009. Cenozoic evolution of the Nile basin. In: Dumont, H.J. (Ed.), The Nile. Monographiae Biologicae, 89, Springer, Dordrecht, 37-60.

Talbot, M.R., Williams, M.A., Adamson, D.A., 2000. Strontium isotope evidence for late Pleistocene reestablishment of an integrated Nile drainage network. Geology 28, 343-346.

Usai, D., 2021. From foraging to food producing: The Mesolithic and Neolithic of the Middle Nile valley. In: Emberling, G., Williams, B., (Eds.), Oxford Handbook of Ancient Nubia, Oxford University Press, pp. ??

Varadzinová, L., Varadzin, L., Garcea, E., Kapustka, K., Řídký, J., Sůvová, Z., Juřičková, L., 2017. Sabaloka (West Bank) Research Project. Exploration of the site of Sphinx (SBK.W-60): 23 findings of the 2014 and 2015 field seasons, Sudan & Nubia 21, 23-49.

Verpoorte, A., 2001. Places of art, traces of fire: A contextual approach to anthropomorphic figurines in the Pavlovian (Central Europe, 29-24 kyr BP). Archaeological Studies of Leiden University 8, Leiden.

Vitali, V., Franklin, U., 1986. New approaches to the characterization and classification of ceramics on the basis of their elemental composition. Journal of Archaeological Science 13, 161-170.

Whitbread, I.K., 1986. The characterisation of argillaceous inclusions in ceramic thin sections. Archaeometry 28, 79-88.

Whitbread, I.K., 1989. A proposal for the systematic description of thin sections towards the study of ancient ceramic technology. In: Maniatis, Y. (Eds.), Proceedings of the 25th International Symposium of Archaeometry. Elsevier, Amsterdam, 127-138.

Whitbread, I.K., 1995. Greek transport of amphorae – A petrological and archaeological study. British School at Athens, Fitch laboratory occasional paper, 4.

825 Whiteman, A.J., 1971. The Geology of the Sudan Republic. Clarendon Press, Oxford University
826 Press, London.
827
828 Wiegand, B.A., 2017. Isotope analysis. In: Hunt, A.M.W., (Ed.), The Oxford Handbook of
829 Archaeological Ceramic Analysis. Oxford University Press, Oxford, pp. 305-326.
830
831 Williams, M.A.J., Adamson, D., Cock, B., McEvedy, R., 2000. Late Quaternary environments in the
832 White Nile region, Sudan. Global and Planetary Change, 26, 305-316.
833
834 Williams, M.A.J., Faure, H., 1980. The Sahara and The Nile: Quaternary Environments and
835 Prehistoric Occupation in Northern Africa. A.A. Balkema, Rotterdam.
836
837 Williams, M.A.J., Jacobsen, G.E.A., 2011. A wetter climate in the desert of northern Sudan 9900–
838 7600 years ago. Sahara 22, 7-14.
839
840 Williams, M.A.J., Talbot, M., Aharon, P., Salaam, Y.A., Williams, F., Brendeland, K.I., 2006. Abrupt
841 return of the summer monsoon 15,000 year ago: new supporting evidence from the lower White
842 Nile valley and Lake Albert. Quaternary Science Review 25, 2651-2665.
843
844 Williams, M.A.J., Usai, D., Salvatori, S., Williams, F.M., Zerboni, A., Maritan, L., Linseele, V., 2015.
845 Late Quaternary environments and prehistoric occupation in the lower White Nile valley, central
846 Sudan. Quaternary Science Reviews 130, 72-88.
847
848 Woodward, J., Macklin, M., Fielding, L., Millar I., Spencer, N., Welsby, D., Williams, M., 2015.
849 Shifting sediment sources in the world's longest river: a strontium isotope record for the Holocene
850 Nile. Quaternary Science Reviews 130, 124-140.
851
852 Woodward, J.C., Macklin, M.G., Krom, M.D., Williams, M.A.J., 2007. The Nile: evolution,
853 Quaternary river environments and material fluxes. In: Gupta, A. (Ed.), Large Rivers:
854 Geomorphology and Management. John Wiley and Sons, Chichester, UK, pp. 261-292.
855

856 Xu, X., Zhang, C., Goldberg, P., Cohen D., Pan, Y., Arpin, T., Bar-Yosef, O., 2012. Early pottery at
857 20.000 years ago in Xianrendong Cave, China. Science 336, 1696-1700.
858
859 Zerboni, A., 2011. Micromorphology reveals in situ Mesolithic living floors and archaeological
860 features in multiphase sites in central Sudan. Geoarchaeology: An International Journal 26, 365-
861 391.
862
863 Zerboni, A., Brandolini, F., Mariani, G.S., Perego, A., Salvatori, S., Usai, D., Pelfini, M., Williams,
864 M.A.J., in press. The Khartoum-Omdurman conurbation: a growing megacity at the confluence of
865 the Blue and White Nile Rivers. Journal of Maps.
866

867 **Figure captions**

868

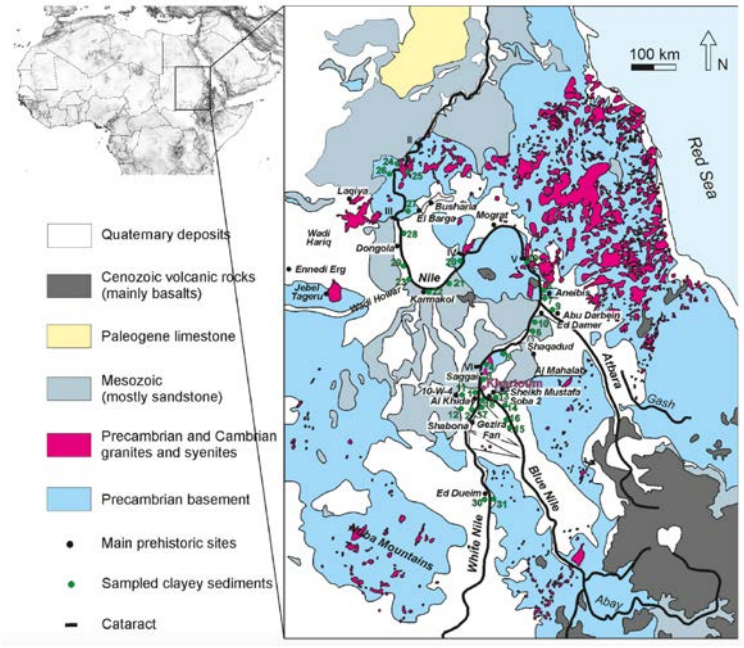

869

870 Figure 1. Geological sketch of Sudan (after Ministry of Energy & Mining, Geological Research
871 Authority of Sudan, 2004) reporting the location of the clayey sediments sampling points
872 (numbers, according to the list reported in Table 1) and of the main prehistoric sites (according to
873 Salvatori and Usai 2019).

874

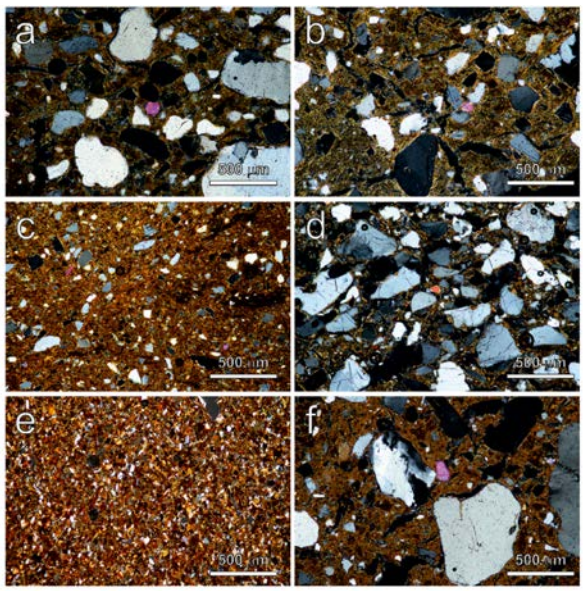

875

876

877 Figure 2. Photomicrographs in crossed-polarized light of clayey materials collected along the White
878 Nile (WN) and Blue Nile (BN): a) 30 (WN); b) 31 (WN); c) 1 (WN); d) 2 (WN); e) 13 (BN); f) 15 (BN).
879 See clay sampling points in Fig. 1 and Table 1.

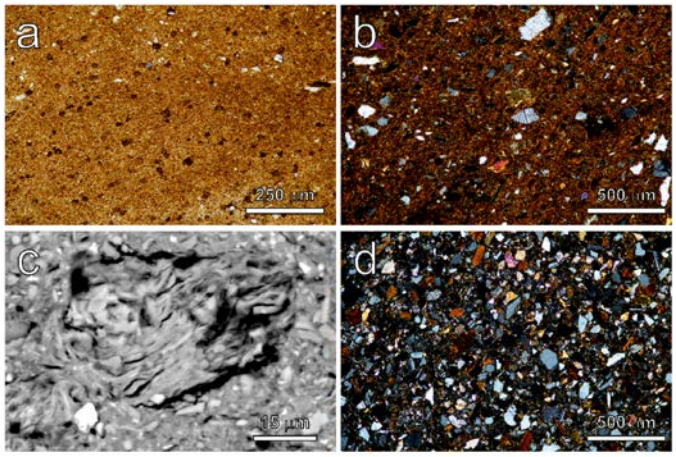

Figure 3. Photomicrographs in crossed-polarized light (a, b, d) and SEM back scattered electron image (c) of clayey materials collected along the Main Nile (MN1) and the river Atbara (A): a) 4; b) 6B; c) detail of a montmorillonite aggregate formed by weathering of a fragment of volcanic mafic rock; d) 9 (A)

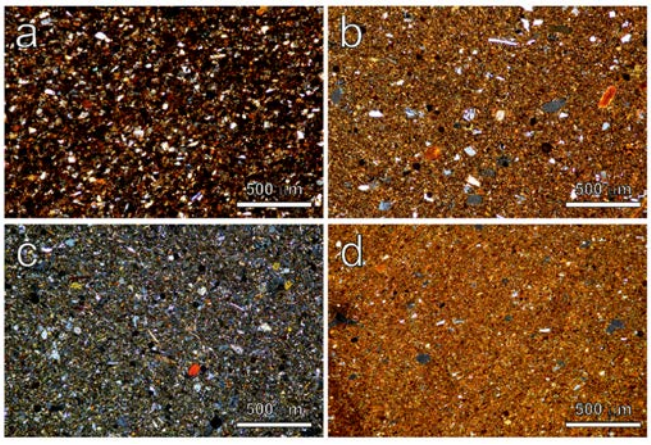

Figure 4. Photomicrographs in crossed-polarized light of clayey materials collected along the Main Nile (MN2), after the confluence of the river Atbara: a) 8; b) 21; c) 28; d) 24.

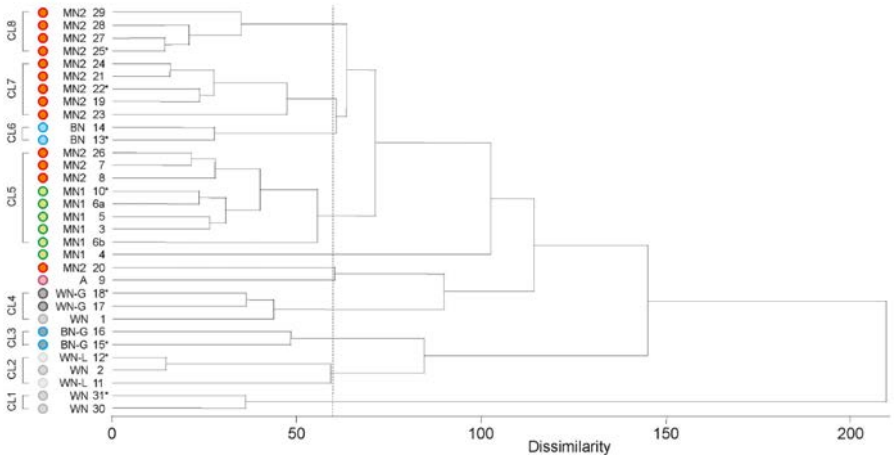

Figure 5. Dendrogram from the cluster analysis performed on XRPD data of clayey materials from the Main Nile 1 (MN1) and 2 (MN2), Atbara (A), White Nile (WN) and related Pleistocene lake and small Holocene ponds (WN-L), Blue Nile (BN), collected also in the Gezira Plain (-G). Statistical analysis was performed according to Euclidean distance and average linkage method, on position and intensity of peaks. The dissimilarity threshold used to define the number of clusters was calculated with the KGS test, according to the software procedure (see Maritan et al., 2015). *: most representative samples within each cluster.

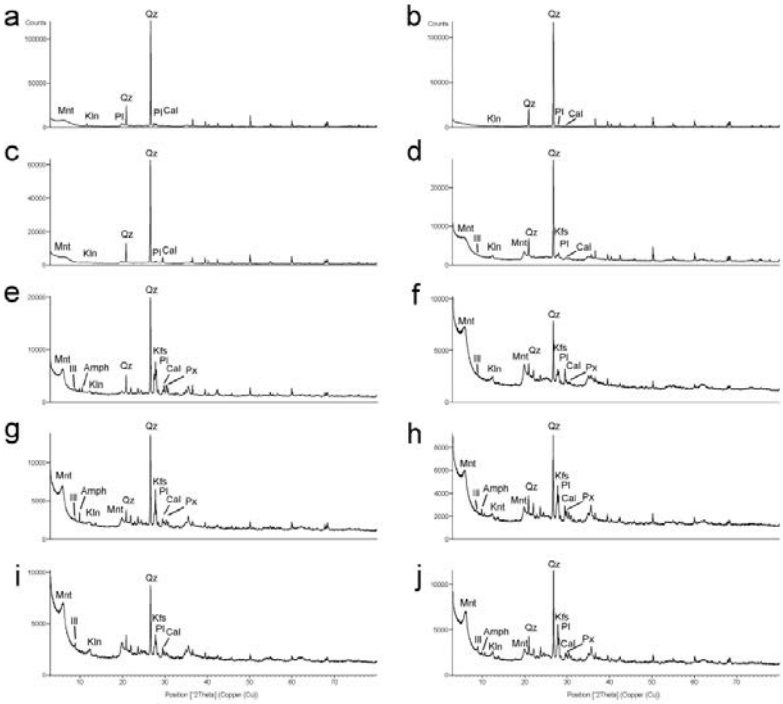

Figure 6. XRPD patterns of the most representative samples of the clusters defined in the dendrogram of the cluster analysis of Fig. 5, and some of the outliers: a) 31; b) 12; c) 15; d) 18; e) 9; f) 4; g) 10; h) 13; i) 22; l) 25. Abbreviations: Qz: quartz; Pl: plagioclase; Kfs: K-feldspar; Cal: calcite; Ill: illite/muscovite; Kln: kaolinite; Amp: amphibole; Mnt: montmorillonite; Px: pyroxene.

905

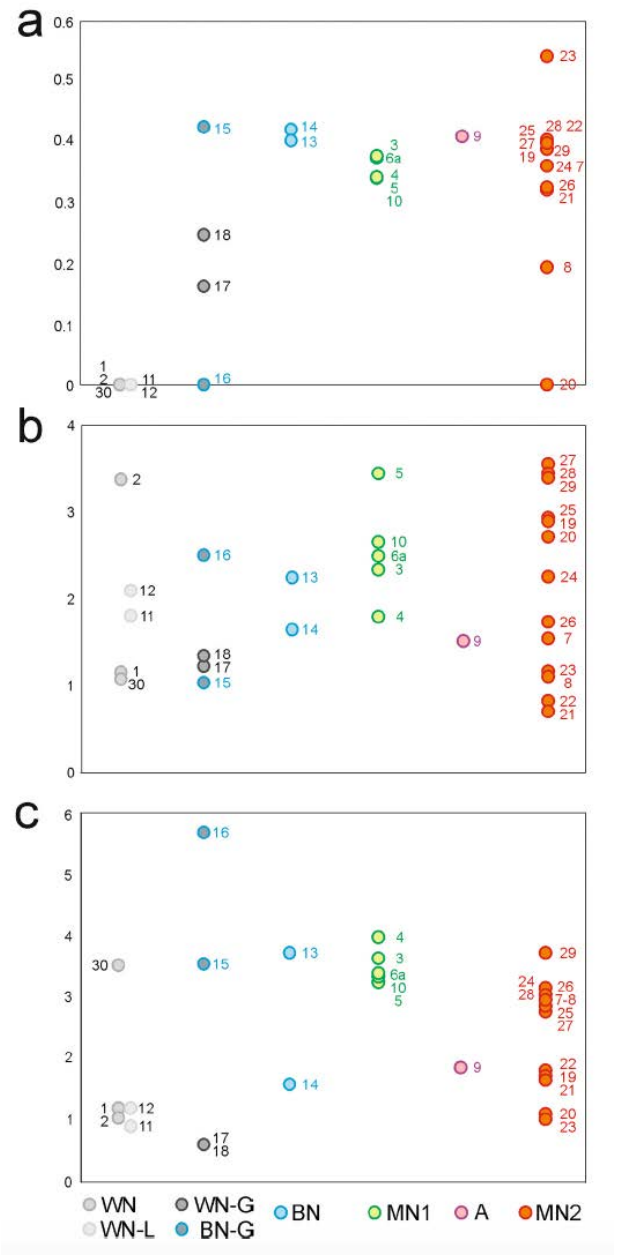

906

907 Figure 7. Plot, according to the hydrographic basin of collection, of: a) interlayer water divided by

908 total (interlayer and structural) water of clay minerals; b) organic matter content (wt%); c) calcite

909 content (wt%) all defined on the basis of the thermal analysis.

910

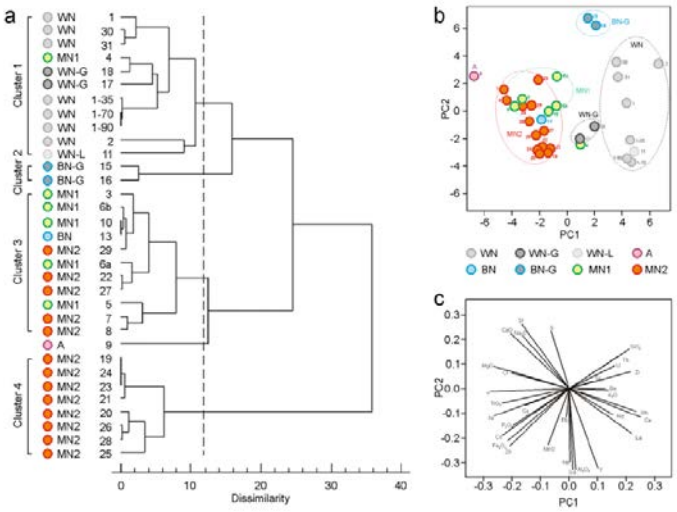

Figure 8: a) Dendrogram obtained from the cluster analysis (Square Euclidean Distance, Ward's method) of log-transformed chemical data, divided by Al_2O_3 (the element with the lowest value of variance (τ.i)); b-c) score and loading plots of PC1 e PC2 obtained by the principal component analysis of the chemical data with indication of the clay number and hydrographic basin from which they were collected. PC1 and PC2 represent the 37% and 23% of the total variance respectively. Abbreviations: WN: White Nile; WN-L: Pleistocene lake and small Holocene ponds and Nubian Sandstone area; BN: Blue Nile; MN1: Main Nile 1; MN2: Main Nile 2; A: Atbara (A); -G: Gezira Plain.

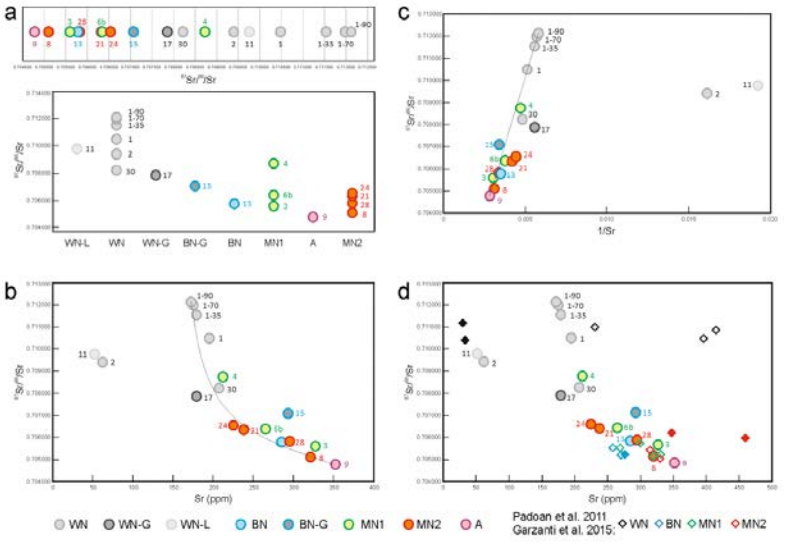

Figure 9. a) $^{87}Sr/^{86}Sr$ distribution according to the hydrographic basin; b) biplot of $^{87}Sr/^{86}Sr$ vs. Sr (ppm); c) biplot of $^{7}Sr/^{86}Sr$ vs. 1/Sr; d) $^{7}Sr/^{86}Sr$ vs. Sr (ppm) reporting for comparison also the data of mud (silt and clay fractions: <60 μm or <40 μm, represented by empty diamonds) and those of some sands (solid diamonds) of Padoan et al. (2011) and Garzanti et al. (2015). Abbreviations: WN:

White Nile; WN-L: Pleistocene lake and small Holocene ponds; BN: Blue Nile; MN1: Main Nile 1; MN2: Main Nile 2; A: Atbara (A); -G: Gezira plain.

Table captions

Table 1. Chemical composition of major and minor (expressed as wt%) and trace elements (expressed as ppm), loss on ignition (LOI) and $^{87}Sr/^{86}Sr$ ratio and its error of the analyzed clay samples. For each sample was also reported the location of the collection point, its coordinates (latitude and longitude) and the hydrographic basic it belongs to. *: Pleistocene lake and small Holocene ponds described by Williams et al. (2015, 2006), Cremaschi et al. (2007) and Williams and Jacobsen (2011). Samples have been listed based on the hydrographic basin within which they were collected: WN: White Nile; WN-G: White Nile in the Gezira plain (eastern bank); WN-L: White Nile related to Pleistocene lake and small Holocene ponds; BN: Blue Nile; BN-G: Blue Nile on the Gezira bank; MN1: Main Nile 1; MN2: Main Nile 2; A: Atbara.

Table 2. Results of the simultaneous thermal analysis TG-DTG-DSC and FTIR-EGA, reporting the weight loss percent (ΔW %), the temperature of DTG and DSC peaks and the composition of EGA (determined by FTIR) for various thermal interval: 40-200°C for the dehydration of montmorillonite; 200-600°C for the dehydration of the phyllosilicates and decomposition of the organic matter; 600-850°C for the carbonate decarbonation; 850-1050°C for the residual dehydration of phyllosilicates and the polymorphic transformation and sintering. Abbreviations: a = endothermic reaction; b = exothermic reaction; ΔW = weight loss; HW: hygroscopic water; IW: inter-layer water; OM: organic matter; DW: dehydroxylation of phyllosilicates. Samples have been listed based on their hydrographic basin: WN: White Nile; WN-G: White Nile in the Gezira plain (eastern bank); WN-L: White Nile related to Pleistocene lake and small Holocene ponds; BN: Blue Nile; BN-G: Blue Nile on the Gezira plain; MN1: Main Nile 1; MN2: Main Nile 2; A: Atbara.